GA–A26237

VALIDATION OF GYROKINETIC TRANSPORT SIMULATIONS USING DIII-D CORE TURBULENCE MEASUREMENTS

by
C. HOLLAND, R.E. WALTZ, J. CANDY, G.R. McKee, M.W. SHAFER, A.E. WHITE,
L. SCHMITZ, and G.R. TYNAN

OCTOBER 2008

GENERAL ATOMICS

DISCLAIMER

GA–A26237

VALIDATION OF GYROKINETIC TRANSPORT SIMULATIONS USING DIII-D CORE TURBULENCE MEASUREMENTS

by
C. HOLLAND,* R.E. WALTZ, J. CANDY, G.R. McKee,† M.W. SHAFER,† A.E. WHITE,‡
L. SCHMITZ,‡ and G.R. TYNAN*

This is a preprint of a paper to be presented at the 22nd IAEA Fusion Energy Conference, October 13-18, 2008, in Geneva, Switzerland, and to be published in the *Proceedings.*

*University of California-San Diego, La Jolla, California.
†University of Wisconsin-Madison, Madison, Wisconsin.
‡University of California-Los Angeles, Los Angeles, California.

Work supported in part by
the U.S. Department of Energy
under DE-FG02-07ER54917, DE-FG03-95ER54309,
DE-FG02-89ER53296, and DE-FG03-01ER54615

GENERAL ATOMICS PROJECT 30200
OCTOBER 2008

GENERAL ATOMICS

Validation of Gyrokinetic Transport Simulations Using DIII-D Core Turbulence Measurements

C. Holland 1), R.E. Waltz 2), J. Candy 2), G.R. McKee 3), M.W. Shafer 3), A.E. White 4), L. Schmitz 4), and G.R. Tynan 1)

1) University of California, San Diego, California, USA
2) General Atomics, San Diego, California, USA
3) University of Wisconsin-Madison, Wisconsin, USA
4) University of California, Los Angeles, California, USA

e-mail contact of main author: chholland@ucsd.edu

Abstract. It is now widely recognized that the development of a predictive modeling capability for ITER and beyond requires the validation of transport codes against experimental measurements at multiple levels. Towards this end, the first direct comparisons of drift-wave turbulence amplitudes, power spectra, and correlation lengths predicted by the gyrokinetic code GYRO against experimental observations are presented. Both local and non-local fixed-gradient simulations are used in this study, while the experimental measurements were obtained in a series of repeatable, steady low-power L-mode discharges. Spatially localized measurements of density fluctuations were obtained via beam emission spectroscopy, and similarly localized measurements of electron temperature fluctuations were obtained via a newly implemented correlation electron cyclotron emission diagnostic on DIII-D. The development and use of synthetic diagnostics to conduct accurate comparisons between experiment and simulation is described in detail. Using these newly implemented synthetic diagnostics with local, fixed-gradient simulations, good agreement between GYRO and experiment is found for fluctuation amplitudes, power spectra, and correlation lengths at normalized toroidal flux $\rho = 0.5$, in addition to close agreement with energy flows calculated via the ONETWO code. At $\rho = 0.75$, flows and fluctuation levels are under predicted by a factor of 7 and 3, respectively, but very good agreement in correlation functions and power spectra "shapes" is still found. To address the issue of profile stiffness, comparisons using results from the new TGLF and TGYRO codes are presented.

1. Introduction

In the absence of large-scale magnetohydrodynamic instabilities, the performance of current magnetic confinement based fusion energy experiments is generally limited by the turbulent transport of particles and energy. It is now generally accepted that this turbulence consists of a broad spectrum of small-scale (i.e. with radial correlation lengths l_r much smaller than the minor radius a of the device) drift-waves driven by the inherent free energy gradients of the confined plasma [1]. Furthermore, it is expected that this drift-wave turbulence will remain a limiting factor for ITER and other future burning plasma devices. Therefore, one must use validated first-principles based models of this turbulence in order to predict the performance of ITER with confidence. Validation is the process by which it is determined that a given computational (or analytic) model accurately represents the stipulated physical processes of interest [2]. This process is separate from verification, which assesses whether a given numerical algorithm yields a sufficiently accurate solution of the model of interest, without reference to the adequacy of that model in representing the physical processes of interest. A key component of the validation process is testing the model in question at multiple levels in a "primacy hierarchy," which ranks different comparisons between model and experiment based upon how many measured or modeled quantities must be integrated into the comparison of interest. From this perspective, comparisons of turbulent particle and energy flows predicted by a given turbulence model against the "experimental" values (which are in reality themselves determined via a power balance analysis that uses a combination of experimental

measurements and computed source models) are the least fundamental, and thus least stringent, comparisons. More fundamental would be comparisons of predictions of various characteristics of individual fluctuation fields, such as amplitudes, correlation lengths, and cross-phases between different fields. The most fundamental comparisons would be of bispectral quantities, which directly quantify the underlying nonlinear couplings and interactions of the turbulence.

Recent advances in experimental diagnostics, nonlinear turbulence simulations, and computational power have opened the door to a new level of turbulence model validation. For instance, new and upgraded fluctuation diagnostics on the DIII-D tokamak [3] are now available which allow highly detailed tests of code predictions in the core region (roughly defined as $\rho<0.8$, where ρ is the normalized toroidal flux), where the underlying gyrokinetic model implemented in the turbulence simulations is believed to be fully valid. Equally important are high-accuracy measurements of the equilibrium plasma profiles, especially of the ion temperature and radial electric field. Concurrent with these experimental advances has been significant maturation of the leading gyrokinetic turbulence codes to include a comprehensive set of physics, and increases in available computing power which allow the use of these mature codes with realistic physical parameters. Taking advantage of these advances, we have recently performed an extensive validation study using the GYRO code [4], examining its ability to simultaneously predict turbulent energy flows, fluctuation spectra, and correlation lengths in a basic L-mode plasma. In order to carry out sufficiently accurate comparisons of simulated and measured fluctuation characteristics, we have developed a set of synthetic diagnostic [5–7] post-processing tools, which allows us to account for the specific frequency and wavenumber sensitivities of each diagnostic. We have also begun to develop and test a new fixed-flow approach [8] (as opposed to the tradition fixed-gradient method), in order to address the tendency of "stiff" plasma transport [9] to greatly magnify uncertainties in the experimental profiles and their gradients.

2. Experimental Summary

In order to minimize uncertainties in the experimental data, a series of repeated stationary L-mode DIII-D discharges (shot numbers 128913-128915) were selected. The discharges are documented in detail in White *et al.* [10]. For this study, all experimental data is averaged over 400 ms during which there is no evidence of any MHD activity (e.g. sawtooth oscillations, tearing modes, ELMs, etc.). The plasma configuration was an upper single-null shape, the toroidal field B_ϕ = 2.1 T, plasma current I_p = 1 MA, and line average electron density $\bar{n}_e$ was 2.3×10^{13} cm^{-3}. A single co-injected neutral beam source was used to apply 2.5 MW of heating; no electron cyclotron heating was used. Density fluctuations were measured via beam emission spectroscopy (BES) [11], and electron temperature fluctuations via correlation electron cyclotron emission (CECE) radiometry [10]. Each diagnostic yields spatially localized measurements of long-wavelength ($k_\perp < 2-4$ cm^{-1}, corresponding to $k_\perp \rho_s < 0.3 - 0.6$ at normalized toroidal flux ρ=0.5) fluctuations, and can be scanned radially on a shot-to-shot basis, yielding profiles of fluctuation characteristics through repeated discharges. The BES system consists of a 5×6 array of channels in the (R, Z) plane which allows measurement of density correlation functions, whereas the initial implementation of the CECE diagnostic on these experiments consists of only two channels which must be cross-correlated to yield a single point measurement of the local electron temperature fluctuation

spectrum. A power balance analysis of the experiment was performed with the ONETWO code [12] to predict ion and electron energy flows (specified in MW, and denoting the total amount of energy flowing across a given magnetic flux surface) for comparison with the GYRO results. We use flows rather than fluxes or diffusivities in these comparisons to eliminate any uncertainties from definitions (e.g. we do not break the flows up into convective and conductive components), or from uncertainties in the profile gradients. We also do not call the ONETWO results the "experimental" flows as is often done, to emphasize that these flows are not measured but rather are the output of a set of complex computational models with their own inherent assumptions and uncertainties. In these shots the magnitude of the wall recycling particle source is essentially unknown and so an accurate experimental value for the particle flow cannot be obtained. We therefore do not attempt to compare the GYRO-predicted particle flow against the ONETWO prediction.

The turbulence in this discharge was modeled with the gyrokinetic initial value code GYRO [4]. GYRO is a massively parallel nonlinear Eulerian *δf* code that solves the coupled gyrokinetic-Maxwell equations. It is the most physically comprehensive code of its sort in use, allowing for an arbitrary number of kinetic ion species, implements a realistic magnetic geometry via a generalized Miller model [13], accepts experimentally measured equilibrium profiles as inputs (including a self-consistent description of the equilibrium $\vec{E}\times\vec{B}$ velocity shear), and includes pitch-angle scattering of electrons and ions. The code can be operated in either a global or local (the $\rho^* \to 0$ limit of the gyrokinetic equation) mode; both approaches were used in this work.

Comparisons of energy flows predicted by a set of local nonlinear GYRO simulations and the values predicted by the power balance analysis are shown in Table I. Each of the simulations used 16 toroidal modes n with a spacing Δn between 2 and 12 (i.e. $n_l = l\Delta n$, $0 \le l \le 15$), selected such that the range in normalized binormal wavenumber $k_y\rho_s$ was between 0 and 1 (where $k_y = nq/r$, r is the midplane minor radius, $q = rB_\varphi/RB_\theta$, $\rho_s = c_s/\Omega_{ci}$, and $c_s = \sqrt{T_e/M_i}$). All simulations were electromagnetic, used a realistic mass ratio $\sqrt{M_i/m_e} = 60$, and included electron collisions. Further details of the simulations can be found in Ref. 7. As can be seen from Table I, the level of agreement obtained between simulation and experiment varies significantly, although we emphasize that this comparison does not accurately account for stiffness of the transport, which significantly magnifies the experimental profile gradient uncertainties. The most important features of the data shown in Table I are the quite good level of agreement at ρ=0.5, and the systematic decrease in GYRO predictions of the energy flows at larger radii, which is opposite the trend seen in the ONETWO flows. For comparison with these results, we note that the GYRO simulations discussed in Ref. [9] of a different 2.1 T L-mode discharge predict energy flows within experimental profile uncertainties which are in agreement with the corresponding power balance analysis over the range ρ = 0.3–0.8. Analysis of other discharges is underway to assess how robust the under prediction of energy flows at larger radii is across varying plasma conditions. The uncertainties quoted for simulation results are the standard deviations σ of the box-averaged flows, where $\sigma^2 = \left(Q - \overline{Q}\right)^2$ and the overbar denotes a time average. Note that the standard deviation quantifies the physically meaningful variability of the turbulent system as well as statistical sampling uncertainties. We use it here because in the absence of a generally accepted definition for the number of "turbulent realizations" N contained in the simulation, it represents an upper bound on the statistical uncertainty which would be given by $\sigma/\sqrt{N}$. The issue of experimental profile and power balance uncertainties is addressed in greater

detail in Sec. 4. However, one can make a simple attempt to quantify the impact of profile uncertainties by performing additional simulations in which one or more of the profiles have been artificially varied (usually within experimental uncertainties). For instance, increasing the equilibrium $\vec{E}\times\vec{B}$ shear rate at ρ=0.5 by 20% yields Q_i = 0.98±0.16 MW and Q_e = 0.86±0.12 MW, even closer to the experimental values. Conversely, decreasing the $\vec{E}\times\vec{B}$ shear rate by 20% at ρ=0.75 yields Q_i = 0.22±0.031 MW and Q_e = 0.23±0.026 MW, still significantly smaller than the experimental values.

TABLE I. Local GYRO Simulation and ONETWO Predictions of Q_i and Q_e.

	ρ=0.21	ρ=0.35	ρ=0.51	ρ=0.64	ρ=0.75
ONETWO Q_i (MW)	0.30	0.65	0.93	1.1	1.1
GYRO Q_i (MW)	0.00	1.0±0.10	1.1±0.17	0.48±0.068	0.16±0.30
ONETWO Q_e (MW)	0.15	0.40	0.74	1.00	1.30
GYRO Q_e (MW)	0.00	0.71±0.071	0.97±0.14	0.46±0.060	0.17±0.023

3. Implementation and Application of Synthetic Diagnostics

In order to move beyond the comparisons of energy flows to a more fundamental level of validation, it is necessary to compare predictions of individual fluctuation field characteristics such as amplitudes, correlation lengths, cross-phases etc. against experimental measurements. In order to make sure comparisons are as accurate as possible, one must use synthetic diagnostics which model what the physical diagnostics in question would have measured, if they had observed the turbulent fields predicted by the simulation. Towards this end, we have developed synthetic BES and CECE diagnostics that can be used to post-process GYRO results. Their implementation is described in greater detail in Ref. [7]. These synthetic diagnostics consist of first applying a mode-number dependent phase shift to translate the GYRO output from a reference frame co-rotating with a particular reference flux surface to the lab reference frame of the diagnostics, and then convolving the relevant lab-frame GYRO fluctuation field with a point spread function (PSF) that models the small but finite volume in physical space over which a given diagnostic channel collects information from. Mathematically, this procedure can be expressed as:

$$\delta X^{LF}\left(r,\theta,\varphi_0,t\right) = \sum_{l=-N_n}^{N_n} \delta\hat{X}_l\left(r,\theta,t\right) e^{-il\Delta n\left[\varphi_0+\nu\left(r,\theta\right)+\omega_0 t\right]} \quad . \tag{1}$$

$$\delta X^{syn}\left(r_0,\theta_0,\varphi_0,t\right) = \frac{\int_{r_{\min}}^{r_{\max}}\int_{-\pi}^{\pi} dr d\theta\ \delta X^{LF}\left(r,\theta,\varphi_0,t\right)\psi\left(r,\theta\right)}{\int_{r_{\min}}^{r_{\max}}\int_{-\pi}^{\pi} dr d\theta\ \psi\left(r,\theta\right)} \quad . \tag{2}$$

Here $\delta\hat{X}_l\left(r,\theta,t\right)$ are the complex plasma-frame toroidal mode amplitudes output by GYRO, φ_0 is the reference toroidal angle at which the comparison is carried out, $\nu\left(r,\theta\right)$ is the phase eikonal (approximately equal to $-q\theta$ in $\hat{s}-\alpha$ geometry), $\omega_0 = -qcE_r/rB$ is the equilibrium rotation frequency, $\psi\left(r,\theta\right) = \psi\left[R\left(r,\theta\right)-R_0, Z\left(r,\theta\right)-Z_0\right]$ is the relevant PSF for a diagnostic channel centered at (R_0, Z_0), and δX^{syn} is the generated synthetic timetrace. This procedure is applied to the simulation at each timepoint of interest (all simulation data is saved every a/c_s,

equivalent to 2–4 ms of physical time), yielding a set of synthetic timetraces which can then be analyzed in the same way as the experimental data. The actual code implementation also records the "unfiltered" signal $\delta X^{LF}(r_0,\theta_0,\varphi_0,t)$ which allows us to quantify the effect of the PSFs. Note that generally a temporal interpolation is applied to the plasma frame data before applying these two transformations, in order to prevent aliasing of the lab-frame spectra from occurring.

We have applied these synthetic diagnostics to the simulations at ρ=0.5 and 0.75, in order to test the GYRO fluctuation predictions, both when the energy flows are well-matched, and when they are not. Contours of the BES and CECE PSFs overlaid on the relevant fluctuation fields are shown in Ref. [7]. In both cases we find that while both PSFs have characteristic sizes comparable to the turbulent eddies, they are also both large enough to significantly attenuate larger wavenumbers. This effect can be seen in Fig. 1, which compares lab-frame power spectra calculated from the unfiltered timetraces (black), the synthetic data (red), and the experimental measurements (blue). All spectra shown are cross-spectra $S(f) = \langle \delta X_1^*(f)\delta X_2(f)\rangle$, calculated between poloidally adjacent BES channels and radially adjacent CECE channels. At ρ=0.5, we observe excellent agreement between the synthetic and experimental BES spectra in both shape and magnitude, and fairly good agreement in the CECE spectra as well. We can quantify the agreement in magnitude by integrating the spectra over the range for 40–400 kHz (set by diagnostic limitations) and defining the root mean square amplitude as $\delta X_{RMS} = \sqrt{\int_{40}^{400} df S(f)}$, the results of which are shown in Table II. At ρ=0.75 we observe significant under predictions of the fluctuation amplitudes. Interestingly, the magnitude of this under prediction is consistent with the under prediction of the flows, as one generally observes turbulent transport to generically scale with fluctuation amplitude squared. Thus, one would expect the under prediction of the flows by a factor of 7 to lead to an under prediction of fluctuation amplitudes by a factor $\sqrt{7} = 2.64$, close to the observed factor of 3. An even more interesting result can be found by rescaling the fluctuation spectra at ρ=0.75 to contain the same amount of power in the 40–400 kHz region as the experimental spectra [shown in purple in Fig. 1(c,d)]. With this rescaling, we observe a remarkable level of agreement between the renormalized synthetic and experimental BES spectra, and between the synthetic and experimental CECE spectra at higher frequency. The source of the mismatch in CECE spectral shapes below 40 kHz remains under investigation. Noting that the mean plasma rotation leads to a significant Doppler shift, one can closely correlate lab-frame frequency with poloidal wavenumber. Therefore, this agreement in spectral shapes should also manifest as good agreement in poloidal correlation function.

Radial and vertical (approximately poloidal) density correlation functions calculated using the simulated and experimental BES data are shown in Fig. 2. As with the spectra, the unfiltered correlation functions are shown in black, the synthetic results in red, and experimental results in blue. Uncertainties are calculated by dividing the array into an "ensemble" of six rows or five columns as appropriate, averaging the results for mean values, and using standard deviations for the uncertainties. Solid curves are fits to the data, using either a Gaussian of the form $\exp\left[-\left(\Delta R/L_R\right)^2\right]$ for the radial correlations, or $\cos\left(2\pi k_0 \Delta Z\right) * \exp\left[-\left(\Delta Z/L_Z\right)^2\right]$ for the vertical correlation functions. As expected from the renormalized spectra comparison, we observe relatively good agreement in the vertical correlation function at ρ=0.75 [Fig. 2(d)]. The other striking features are the impact of the PSFs on the radial correlation functions (evidenced by the differences in the black and red

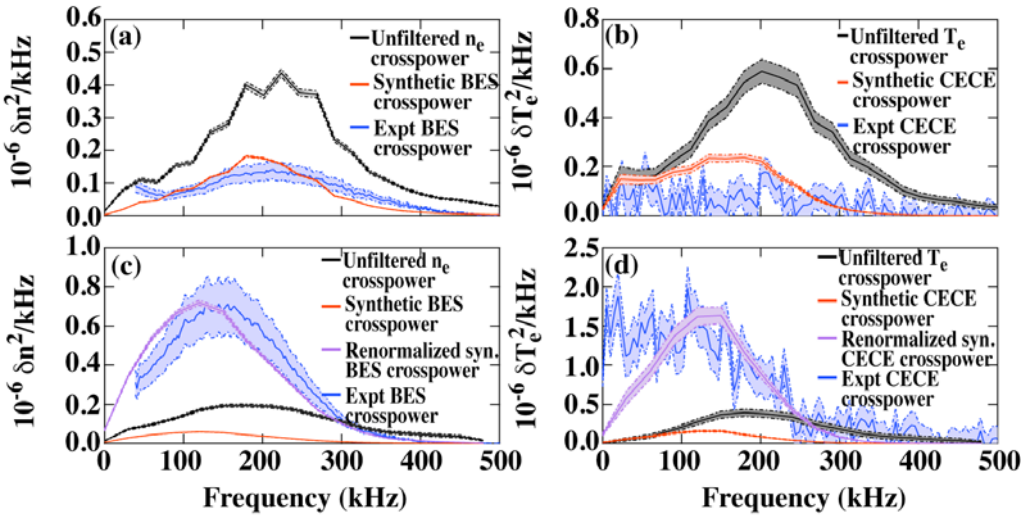

FIG. 1. Lab-frame cross-spectra of δn_e (a,c) and δT_e (b,d) from local GYRO simulations of ρ=0.5 (a,b) and ρ=0.75 (c,d). Spectra calculated from the unfiltered GYRO data are shown in black, from the synthetic BES data in red, and from the experimental data in blue.

TABLE II. Comparison of GYRO-predicted and Experimental RMS Fluctuation Amplitudes.

	Unfiltered RMS δn	Synthetic RMS δn	Experimental RMS δn	Unfiltered RMS δT_e	Synthetic RMS δT_e	Experimental RMS δT_e
ρ=0.50	$0.90\pm1.5\times10^{-2}$	$0.55\pm7.7\times10^{-3}$	0.56±0.11	$1.1\pm5.7\times10^{-2}$	$0.66\pm2.4\times10^{-2}$	0.46±0.22
ρ=0.75	$0.69\pm1.9\times10^{-2}$	$0.33\pm6.9\times10^{-3}$	1.10±0.22	$1.9\pm7.7\times10^{-2}$	$0.5\pm1.9\times10^{-2}$	1.60±0.24

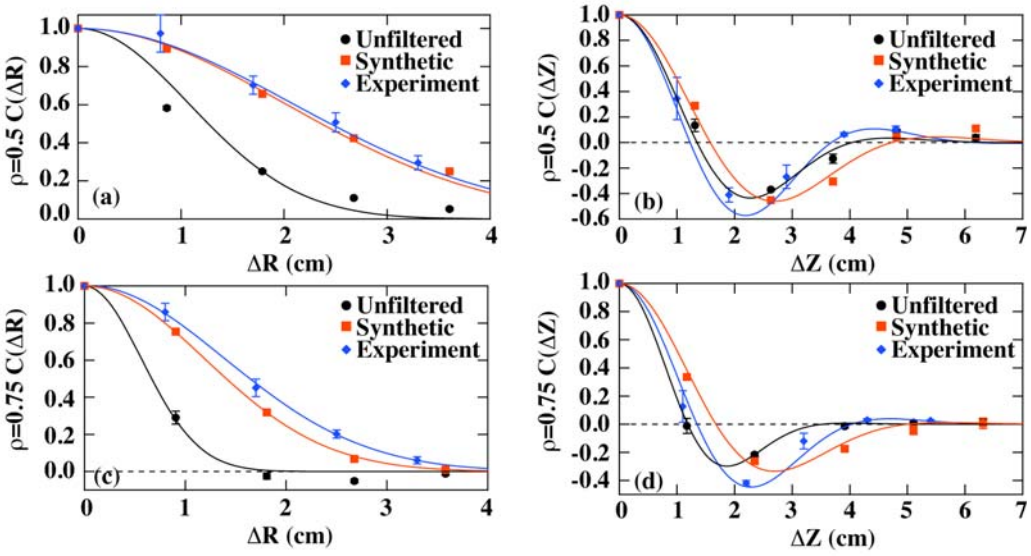

FIG. 2. Radial (a,c) and vertical (b,d) density correlation functions from local GYRO simulations of ρ=0.5 (a,b) and ρ=0.75 (c,d). Correlation functions calculated from the unfiltered GYRO data are shown in black, from the synthetic BES data in red, and from the experimental data in blue. The solid curves are Gaussian fits to the data (with an additional mean wavenumber allowed for in the vertical correlation functions).

curves, Fig. 3(a,b)], and by the overall level of agreement between the synthetic and experimental results at both locations and in both directions. Combined with the comparisons of fluctuation amplitude and frequency power spectra shape, we can state that GYRO appears

to accurately reproduce the measured fluctuation characteristics at ρ=0.5 as well as the energy flows, while at ρ=0.75 it appears to reproduce the spatial structure of the turbulence correctly even though it significantly under predicts the fluctuation and energy flow levels. The reason for this under prediction remains unclear, and will be the subject of future work. Some possible explanations are discussed in Ref. [7].

4. Fixed-Flux Simulation Results

It is well known that the turbulent transport associated with drift-waves is "stiff," such that small changes in the local free energy gradients can yield large changes in the flows [9]. Although one can generally find good fits to sets of point measurements of equilibrium profiles via splining, the resulting curves are not unique, and so there are significant systematic uncertainties in such fits, even when statistical uncertainties have been minimized. Because these systematic profile uncertainties translate into even larger uncertainties in the flows predicted by traditional fixed-gradient simulations such as those described above, the validation value of such simulations is distinctly limited. One way in which this issue can be addressed is to take the next step in predictive transport modeling and use fixed-flow simulations, in which a "transport driver" code adjusts the background plasma profiles until the flows predicted by the simulation match the flows predicted by power balance analysis of the particle and heating sources.

Our first effort in this direction was to use the quasilinear TGLF model [14,15] to predict equilibrium T_i and T_e profiles necessary to match the ONETWO power balance analysis, shown in blue in Fig. 3(a,b) (the density profile was held constant). We then performed a global fixed-gradient GYRO simulation using these TGLF-predicted profiles, shown in blue in Fig. 3(c,d). These results should be contrasted with the results of a global GYRO simulation that uses the same spline-fitted equilibrium profiles as the ONETWO analysis (all

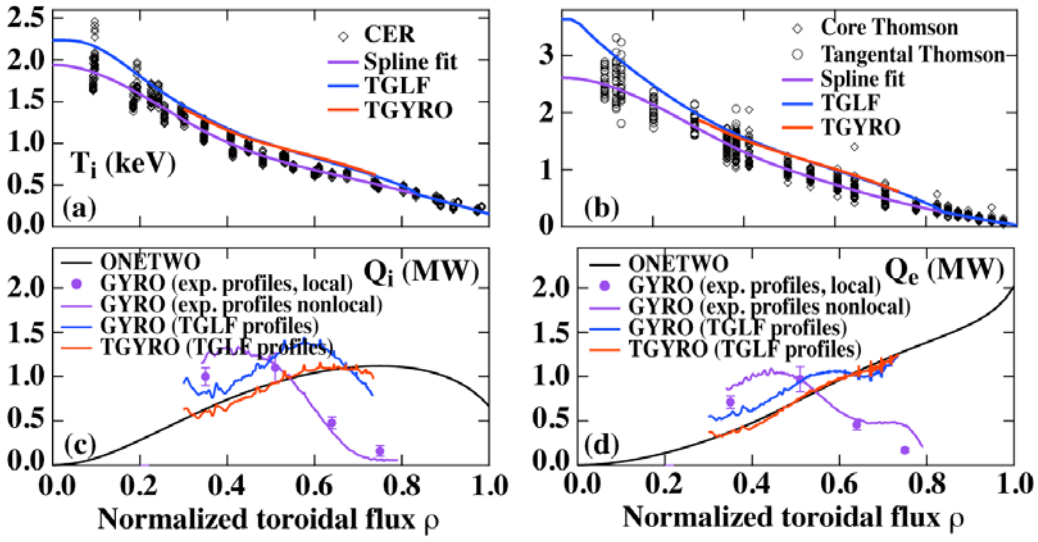

FIG. 3. Equilibrium T_i (a) and T_e (b) profiles calculated as spline fits (purple) to the measured data (black), as well as the TGLF flow-matching profiles (blue) and TGYRO adjustments to those profiles (red). The corresponding energy flows are shown in (c) and (d). ONETWO calculations using the spline fits are shown in black, GYRO results using the spline fits in purple (global results as solid lines, and local results as individual points), GYRO results using the TGLF profiles in blue, and TGYRO results starting from the TGLF profiles in red.

shown in purple in Fig. 3). We also plot the local GYRO simulations discussed in Sec. 2 and 3 as individual purple points, demonstrating good agreement at all locations between the global and local results. Turning back to the TGLF results, the main conclusion which can be drawn is that significantly improved agreement in the energy flows can be achieved by increasing the magnitude of T_i and T_e inside the TGLF pivot point at ρ=0.85, particularly T_e. The magnitude of this increase is large enough to likely be outside what would be considered a good fit to the data. How best to quantify this disagreement relative to the disagreement in flows obtain by the initial fixed-gradient simulations remains an open question.

We can improve the agreement in fluxes even further by using the TGLF-predicted profiles as inputs to the TGYRO code [8], which adjusts the local T_i and T_e scale lengths at each radial location in the GYRO simulation based upon the mismatch between the power balance and GYRO energy flows. These results are shown in red in Fig. 3, and are the most clear exhibition of profile stiffness. By making small changes to the temperature profiles (such that the blue TGLF and red TGYRO profiles are essentially indistinguishable), one is able to obtain a near-exact match to the ONETWO results. Conversely, initial attempts in using TGYRO with the spline-fit profiles have not yielded a steady solution, with significant changes being made to the profiles at large ρ, while still under predicting the ONETWO analysis by up to a factor of two.

Acknowledgments

This work was supported by the US Department of Energy under DE-FG02-07ER54917, DE-FG03-95ER54309, DE-FG02-89ER53296, DE-FG03-01ER54615, NS53250, and DE-AC05-76OR00033.

References

[1] HORTON, W., Rev. Mod. Phys. **71**, 735 (1999).
[2] TERRY, P.W., *et al.*, Phys. Plasmas **15**, 062503 (2008).
[3] LUXON, J.L., Nucl. Fusion **42**, 614 (2002).
[4] CANDY, J. and WALTZ, R.E., J. Comput. Phys. **186**, 545 (2003). Also see http://fusion.gat.com/theory/Gyro for the most recent documentation.
[5] BRAVENEC, R.V. and NEVINS, W.M., Rev. Sci. Instrum. **77**, 015101 (2006).
[6] ERNST, D.R., *et al.*, Fusion Energy 2006 (Proc. 21st Int. Conf. Chengdu, 2006) (Vienna: IAEA) CD-ROM file TH/1-3.
[7] HOLLAND, C., *et al.*, J. Physics: Conf. Series **125**, 012043 (2008).
[8] WALTZ, R.E., *et al.*, Nucl. Fusion **45**, 741 (2005).
[9] CANDY, J. and WALTZ, R.E., Phys. Rev. Lett. **91**, 045001 (2003).
[10] WHITE, A.E., *et al.*, Phys. Plasmas **15**, 056116 (2008).
[11] McKEE, G.R., *et al.*, Rev. Sci. Instrum. **77**, 10F104 (2006).
[12] ST JOHN, H.E., *et al.*, Plasma Phys. Control. Fusion **3**, 603 (1994).
[13] MILLER, R.L., *et al,* Phys. Plasmas **5**, 973 (1998).
[14] STAEBLER, G.M., KINSEY, J.E., and WALTZ, R.E., Phys. Plasmas **14**, 055909 (2007).
[15] KINSEY, J.E., STAEBLER, G.M., and WALTZ, R.E., Phys. Plasmas **15**, 055908 (2008).